Hindawi
Journal of Engineering
Volume 2018, Article ID 7827324, 11 pages
https://doi.org/10.1155/2018/7827324

Research Article

Effect of Microstructure and Exothermic Reaction on the Thermal Convection in an Enclosure of Nanoliquid with Continuous and Discontinuous Heating from below

Abeer Alhashash

Department of Mathematics, Faculty of Science, Jouf University, 24241 Sakaka Aljawf, Saudi Arabia

Correspondence should be addressed to Abeer Alhashash; dr.abeeralhashash@gmail.com

Received 24 May 2018; Revised 27 July 2018; Accepted 13 August 2018; Published 3 September 2018

Academic Editor: Sergio Nardini

Effect of continuous and discontinuous external heating and internal exothermic reaction on thermal convection of micropolar nanoliquid is studied in the present work. The liquid in the enclosure is a water-based nanoliquid containing Cu nanoparticles. The governing equations are solved numerically using the iterative finite difference method (FDM). The studied parameters are the material viscosity ($0 \le K \le 6$), nanoparticles volume fraction ($0.0 \le \phi \le 0.2$), and the internal heating ($0.0 \le G \le 2.0$). It is found that the convective flow acceleration by adding nanoparticles is retarded by the microrotation and the suppression has a great impact on the weak exothermic reaction for both cases. Increasing the internal reaction decreases the heat transfer rate at the hot wall but increases the heat transfer rate at the cool wall for both cases, Newtonian or micropolar nanoliquid.

1. Introduction

Today electrical machines are commonly used in the industry. It is desirable to have machines which are as small, efficient, and long lasting. To be able to make the machines smaller without reducing the power, it is important to get a better cooling of the machine, preferably by using natural convection. The convection describes the exchange of thermal energy between physical systems depending on the thermal, velocity, and pressure, by dissipating heat. Heat transfer rate could be improved by modifying thermophysical properties of the liquid. Using solid nanoparticles having very high thermal conductivities dispersed in liquid would substantially modify the liquid properties. This technique is proposed by Choi [1] and the new liquid is called nanoliquid. Nanoparticles are basically metal, oxides, and some other compounds such as graphene. This engineered liquids have potential applications, for example, heat exchanger, building construction, micro electromechanical systems, nuclear reactors, geothermal power, solar cells, electronics cooling, and so forth. Khanafer et al. [2] and Jou and Tzeng [3] obtained 25% augmentation in the heat transfer rate with 20% weight fractions of the suspended Cu nanoparticles. The Ag, Cu, CuO, Al_2O_3, or TiO_2 nanoparticles are utilized by Öğüt [4]. They reported 155% augmentation in the heat transfer rate utilizing 20% weight fractions of the Ag nanoparticles. Rashmi et al. [5] filled the enclosure with Al_2O_3 nanoparticle. They reported a reduction in heat transfer rate with an increment percentage of the nanoparticle for a particular heating parameter. Sheikhzadeh et al. [6] considered the Brownian and thermophoresis diffusions and found the heat transfer reduction by increasing the bulk volume fraction of nanoparticles. Boulahia et al. [7] observed that the heat transfer rate increases with decreasing the nanoparticle diameter and the highest values of the heat transfer rate occur at 25nm diameter. Motlaghc and Soltanipour [8] reported about 26% augmentation in the heat transfer rate with 4% weight fractions of the solid nanoparticles. Liao [9] investigated systematically the influence of the Rayleigh number on the heat transfer behavior with increasing Al_2O_3 nanoparticle volume fraction to 6%. He built a correlation equation for reproducing the critical Rayleigh number with the averaged temperature.

Heat transfer performance strongly depends on the media, i.e., liquid. Aydin and Pop [10] and Saleem et al. [11] showed that micropolar liquid give lower heat transfer values than those of the Newtonian liquid. Micropolar liquid is

a subset of the non-Newtonian liquid. It is composed of dumb-bell structural molecules or small and stiff cylindrical components, for example, liquid mixtures, polymer liquid, animal blood, and engine oil. The earlier study of micropolar liquid in enclosures was conducted by Jena and Bhattacharyya [12]. They compared convection stability for several values of micropolar liquid parameters. Wang and Hsu [13] studied the influence of material parameter, geometry aspect ratio, and geometry orientation for the enclosure filled with micropolar liquid at unsteady and stationary conditions. They found that angles of inclination at the maximum values of the heat transfer were coincident for various micropolar liquid in the range of aspect ratio 1.75 to 0.75. Hsu and Chen [14] concluded that thermal performance of a micropolar liquid reduces with the vortex viscosity enhancement and stability of micropolar liquid is higher than that of the stability of Newtonian liquid. A heat sources effect was later included by Hsu et al. [15]. Hsu and Hong [16] investigated the microstructure in an open cavity and found that increasing the Grashof number increases both heat transfer rate and liquid circulation. Gibanov et al. [17] found that an increase in the vortex viscosity parameter leads to attenuation of the convective flow and heat transfer inside a trapezoidal enclosure. Later, Miroshnichenko et al. [18] analyzed the effects of Rayleigh number, Prandtl number, vortex viscosity parameter, and the heater location on streamlines, isotherms, and vorticity profile. Sheremet et al. [19] studied a right-angled wavy triangular enclosure and obtained an essential heat transfer reduction and liquid flow attenuation with vortex viscosity parameter. Turk and Tezer-Sezgin [20] observed that the streamlines and microrotation contours are similar to altering magnitudes. Recently, Ali et al. [21] observed that the expansion of isotherms toward the top boundary surface for greater values of the micropolar parameter and the Nusselt numbers decrease with change in the behavior of the liquid from Newtonian to micropolar.

The vehicle of the current investigation is to study a natural convection heat transfer in a square enclosure filled with micropolar nanoliquid when the bottom boundary is continuously and discontinuously heated at T_h temperature. The top boundary is adiabatic, while the side boundaries walls have constant T_c temperature where $T_c < T_h$. The liquid in the enclosure is a water-based nanoliquid containing Cu nanoparticles. Quadratic heat profile is assumed to be generated internally by the exothermic reaction. An exothermic reaction is a chemical reaction that releases energy by light or heat and the typical application of this process occurs in chemical industry. Similar research conducted by Bourantas and Loukopoulos [22] for continuously heating left wall showed that the microrotation of the nanoparticles decreases heat transfer and should not therefore be neglected when computing heat and liquid flow of micropolar liquid, as nanoliquid. Hashemi et al. [23] and Izadi et al. [24] investigated the copper-water micropolar nanoliquid inside a porous enclosure with continuous heating left wall. The nanoparticles are translating, rotating, and choosing a discontinuous thermal condition along the bottom wall which could have a great impact on the heat transfer rate. Systematical comparison between continuous and discontinuous heating cases is also carried out.

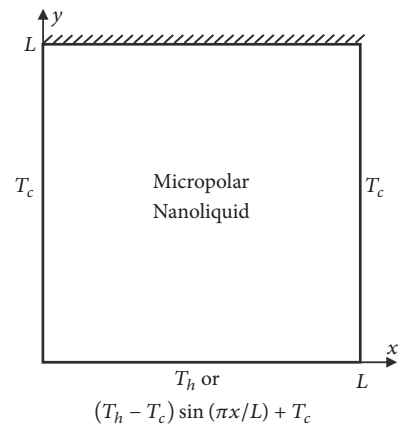

Figure 1: Schematic representation of the model.

2. Mathematical Formulation

A schematic diagram of a square enclosure with micropolar nanoliquid is shown in Figure 1. The liquid in the enclosure is a water-based nanoliquid containing Cu nanoparticles. Quadratic heat profile is generated internally by the exothermic reaction. The bottom boundary is continuously and discontinuously heated while the top boundary is adiabatic and side boundaries walls have constant low temperature. The governing equation is based on conservation laws of mass, momentum, and energy with appropriate rheological models and equations. For micropolar nanoliquid flow the continuity equation, linear momentum equation, angular momentum equation and energy equations are given as follows:

$$\nabla^2 u = -\frac{\partial \omega}{\partial y} \tag{1}$$

$$\nabla^2 v = -\frac{\partial \omega}{\partial x} \tag{2}$$

$$\rho_{nl}\left(\mathbf{u}\cdot\boldsymbol{\nabla}\omega\right) = \left(\mu_{nl}+\kappa\right)\nabla^2\omega - \kappa\nabla^2 N + g\left(\rho\beta\right)_{nl}\frac{\partial\left(T-T_h\right)}{\partial x} \tag{3}$$

$$\rho_{nl} j\left(u\cdot\nabla N\right) = \gamma_{nl}\nabla^2 N - 2\kappa N + \kappa\omega \tag{4}$$

$$u\cdot\nabla T = \alpha_{nl}\nabla^2 T + \frac{\lambda}{\left(\rho Cp\right)_{nl}}\left(T-T_c\right)^2 \tag{5}$$

where subscript nl is nanoliquid, u and v are the velocity components along x and y axes, T is the liquid temperature, N is the component of the microrotation vector normal to the xy plane, g is the magnitude of the acceleration due to gravity, ρ is the density, μ is the dynamic viscosity, κ is the vortex viscosity, γ is the spin-gradient viscosity, j is the microinertia density, and n is a constant with values $0 \le n \le 1$, with $n = 0$, called strong concentration of microelements. Further, we assume that γ_{nl} has the following form:

$$\gamma_{nl} = \left(\mu_{nl} + \frac{\kappa}{2}\right) \tag{6}$$

The viscosity of the nanoliquid can be approximated as viscosity of a base liquid if it contains dilute suspension of fine spherical particles, which is given by Brinkman [25] as

$$\frac{\mu_{nl}}{\mu_{bl}} = \frac{1}{(1-\phi)^{2.5}} \tag{7}$$

where ϕ is the solid volume fraction of nanoparticles. Thermal diffusivity of the nanoliquid is

$$\alpha_{nl} = \frac{k_{nl}}{(\rho Cp)_{nl}} \tag{8}$$

where the heat capacitance of the nanoliquid given is

$$(\rho Cp)_{nl} = (1-\phi)(\rho Cp)_{bl} + \phi(\rho Cp)_{sp} \tag{9}$$

and k_{nl} stands for the effective thermal conductivity of nanoliquid restricted to spherical nanoparticles is approximated by the Maxwell-Garnetss (MG), Öğüt [4] model:

$$\frac{k_{nl}}{k_{bl}} = \frac{k_{sp} + 2k_{bl} - 2\phi(k_{bl} - k_{sp})}{k_{sp} + 2k_{bl} + \phi(k_{bl} - k_{sp})} \tag{10}$$

The thermophysical properties of liquid and the solid copper phases are given by Khanafer et al. [2]. The appropriate the boundary conditions are as follows:

$$u = v = 0 \quad \text{and} \quad \frac{\partial T}{\partial y} = 0 \quad \text{at } y = \ell \tag{11}$$

$$u = v = 0 \quad \text{and} \quad T = T_c \quad \text{at } x = 0 \tag{12}$$

$$u = v = 0 \quad \text{and} \quad T = T_c \quad \text{at } x = \ell \tag{13}$$

$$u = v = 0 \quad \text{and} \quad T = T_h \quad \text{or} \quad T = (T_h - T_c)\sin\left(\frac{\pi x}{\ell}\right) + T_c \quad \text{at } y = 0 \tag{14}$$

The above equations can be cast in nondimensional form by incorporating the following dimensionless parameters:

$$X = \frac{x}{\ell}, \quad Y = \frac{y}{\ell},$$
$$U = \frac{u\ell}{\nu_{bl}}, \quad V = \frac{V\ell}{\nu_{bl}},$$
$$\Theta = \frac{T - T_c}{T_h - T_c}, \quad Pr_{bl} = \frac{\nu_{bl}}{\alpha_{bl}},$$
$$Ra_{bl} = \frac{g\beta_{bl}(T_h - T_c)\ell^3}{\nu_{bl}\alpha_{bl}},$$
$$G = \frac{\lambda(T_h - T_c)l}{\alpha_{bl}(\rho Cp)_{bl}} \tag{15}$$

Writing in stream function–vorticity formulation and performing nondimensionalization, the dimensionless form of the governing equations is expressed as follows:

$$\nabla^2\Psi = -\Omega \tag{16}$$

$$\frac{\partial\Psi}{\partial Y}\frac{\partial\Omega}{\partial X} - \frac{\partial\Psi}{\partial X}\frac{\partial\Omega}{\partial Y} = \left(\frac{\mu_{nl}}{\mu_{bl}} + K\right)\frac{\rho_{bl}}{\rho_{nl}}\nabla^2\Omega - K\frac{\rho_{bl}}{\rho_{nl}}\nabla^2 N + \frac{Ra_{bl}}{Pr_{bl}}\frac{(\rho\beta)_{nl}}{(\rho\beta)_{bl}}\frac{\rho_{bl}}{\rho_{nl}}\frac{\partial\Theta}{\partial X} \tag{17}$$

$$\frac{\partial\Psi}{\partial Y}\frac{\partial N}{\partial X} - \frac{\partial\Psi}{\partial X}\frac{\partial N}{\partial Y} = \left(\frac{\mu_{nl}}{\mu_{bl}} + \frac{K}{2}\right)\frac{\rho_{bl}}{\rho_{nl}}\nabla^2 N - 2K\frac{\rho_{bl}}{\rho_{nl}}N + K\frac{\rho_{bl}}{\rho_{nl}}\Omega \tag{18}$$

$$\frac{k_{nl}}{k_{bl}}\frac{(\rho Cp)_{bl}}{(\rho Cp)_{nl}}\nabla^2\Theta = Pr_{bl}\left(\frac{\partial\Psi}{\partial Y}\frac{\partial\Theta}{\partial X} - \frac{\partial\Psi}{\partial X}\frac{\partial\Theta}{\partial Y}\right) - G\Theta^2 \tag{19}$$

The dimensionless boundary conditions are as follows:

$$\Psi = 0 \quad \text{and} \quad \frac{\partial\Theta}{\partial Y} = 0 \quad \text{at } Y = 1 \tag{20}$$

$$\Psi = 0 \quad \text{and} \quad \Theta = 0 \quad \text{at } X = 0 \tag{21}$$

$$\Psi = 0 \quad \text{and} \quad \Theta = 0 \quad \text{at } X = 1 \tag{22}$$

$$\Psi = 0 \quad \text{and} \quad \Theta = 1 \quad \text{or} \quad \Theta = \sin(\pi X) \quad \text{at } Y = 0 \tag{23}$$

3. Numerical Method and Validation

The governing equations are categorized as elliptical partial differential equation; one of the well-known methods to solve these equations is using iterative finite difference method. Central difference method is utilized for discretizing the first and second derivative of the governing equations while backward difference method is utilized for discretizing the insulated boundary. The finite difference form of equation relating the energy equation (19) is

$$\left(\frac{k_{nl}}{k_{bl}}\frac{(\rho Cp)_{bl}}{(\rho Cp)_{nl}}\right)\left[\frac{\Theta_{i+1,j} - 2\Theta_{i,j} + \Theta_{i-1,j}}{\Delta X^2} + \frac{\Theta_{i,j+1} - 2\Theta_{i,j} + \Theta_{i,j-1}}{\Delta Y^2}\right] = S_{i,j} \tag{24}$$

This can be simplified as

$$\Theta_{i,j} = \frac{1}{2\left(1 + \Delta X^2/\Delta Y^2\right)}\left[\Theta_{i+1,j} + \Theta_{i-1,j} + \frac{\Delta X^2}{\Delta Y^2}\left(\Theta_{i,j+1} + \Theta_{i,j-1}\right) + \Delta X^2\left(\frac{k_{bl}}{k_{nl}}\frac{(\rho Cp)_{nl}}{(\rho Cp)_{bl}}\right)S_{i,j}\right] \quad (25)$$

where

$$S_{i,j} = Pr_{bl}\left[\left(\frac{\Psi_{i,j+1} - \Psi_{i,j-1}}{2\Delta Y}\right)\left(\frac{\Theta_{i+1,j} - \Theta_{i-1,j}}{2\Delta X}\right) - \left(\frac{\Psi_{i+1,j} - \Psi_{i-1,j}}{2\Delta X}\right)\times\left(\frac{\Theta_{i,j+1} - \Theta_{i,j-1}}{2\Delta Y}\right) - G\left(\frac{\Theta_{i+1,j} + \Theta_{i-1,j} + \Theta_{i,j+1} + \Theta_{i,j-1}}{4}\right)^2\right] \quad (26)$$

The computation is assumed to move through the grid points from the east to the west and the south to the north. The finite difference form of equation relating the stream function (16), vorticity (17), and microrotation (18) could be treated in the same way. Good approximation of the vorticity at the boundaries is the most critical step in the stream function-vorticity formulation. The vorticity is calculated by

$$\Omega = -\frac{\left(8\Psi_{1,j} - \Psi_{2,j}\right)}{2\left(\Delta Y\right)^2} \quad (27)$$

Similar expressions are written for the left and right walls. Next, the solutions of the algebraic equations are performed using Gaussian SOR iteration. The unknowns Ψ, Ω, Θ, and N are calculated until the following criterium of convergence is fulfilled:

$$\max\left|\frac{\zeta_{i,j}^{n+1} - \zeta_{i,j}^{n}}{\zeta_{i,j}^{n}}\right| \leq \epsilon \quad (28)$$

where ζ is either Ψ, Ω, Θ, or N and n represents the iteration number and ϵ is the convergence criterion. Finally, the integration of average Nusselt number is done by using the second-order Simpson method. In this study, the convergence criterion is set at $\epsilon = 10^{-6}$. Regular and uniform grid distribution is used for the whole enclosure. The effect of grid resolution was examined in order to select the appropriate grid density as demonstrated in Figure 2 for $K = 4$, $\phi = 0.02$, $Ra = 10^5$, $G = 1.0$ for continuous case 1. Considering the accuracy and the computation time, the results indicate that an 121×121 mesh can be used in the final computations. As a validation, the results (left) of streamlines are compared with that obtained by Aydin and Pop [10] (right) for the continuously heated left wall at $\phi = 0$, $Ra = 10^6$, $Pr = 0.71$, $K = 0, 2$ as shown in Figure 3.

4. Results and Discussion

The reported results are considered for water and the Rayleigh number is set at $Ra = 10^5$. The microrotation contour is not presented in this work. The analysis in the undergoing numerical investigation are performed in the following range of the associated dimensionless groups: the material viscosity ($0 \leq K \leq 6$), the solid particle concentration ($0.0 \leq \phi \leq 0.2$), and the internal heating parameter, $0.0 \leq G \leq 2.0$.

Figure 4 exhibits the influence of the viscosity parameter, K, for continuous heating case and nanoliquid (solid lines) with volume fraction 10% and pure fluid (dashed lines) for $G = 1.0$ on the streamlines and the isotherms. K affects the liquid temperatures and the flow characteristics. An increase in the vortex viscosity parameter reduces the mean velocity, due to increasing of the vortex viscosity on the global viscous effect. The strength of nanoliquid flow circulation is stronger than the strength of base liquid flow circulation at $K = 2$ and $K = 4$. Later, at $K = 6$ the flow acceleration by adding nanoparticles is then retarded by the microrotation effect. The isotherms are focused near the corners of bottom wall for base liquid and nanoliquid irrespective to viscosity parameter. This happened because of the effect of the microstructures nanoliquid; the mean velocity decelerates with the vortex viscosity enhancement. The concentration of microconstituents is enhanced with the raise in K. Thus, big amount of the energy inside the system is consumed in processing rotational speed of the micropolar nanoliquid, and, as a result, the liquid movement from the lower to the top portion is retarded. The chamber in the middle, top surface, is obtained for base liquid at $K = 2, 4, 6$. This is related to the quadratic internal heating from the exothermic reaction.

Figure 5 exhibits the influence of the viscosity parameter, K, for discontinuous heating case 2 and nanoliquid (solid lines) with volume fraction 10% and pure liquid (dashed lines) where $G = 1.0$ on the streamlines and the isotherms. The strength of nanoliquid flow circulation is higher than the strength of base liquid flow circulation at $K = 2$. Later, at $K = 4$, the flow acceleration by adding nanoparticles is then slightly retarded by the microrotation. Afterwards, suppression of the flow circulation by the increasing the vortex viscosity is more pronounced at $K = 6$. The maximum flow strength of continuous heating case depicted in the previous figure is slightly higher than the maximum flow strength of discontinuous heating case for the considered viscosity parameters. The isotherms of base liquid and nanoliquid are found to be distributed sinusoidally for the all material parameter. The streamlines of micropolar base liquid and micropolar nanoliquid are similar and the isotherms of micropolar base liquid and micropolar nanoliquid are deviated in the upper part of enclosure. There are no chambers in the middle, top surface for the base liquid or nanoliquid at $K = 2, 4, 6$. It seems the sinusoidal external heating effect is superior to the exothermic reaction effect.

Tables 1 and 2 present the maximum values of clockwise and counter clockwise flow circulations against internal heating parameter with different K for continuous case 1 and discontinuous case 2, respectively. It is seen from both tables that, for given values of internal heating parameter, the

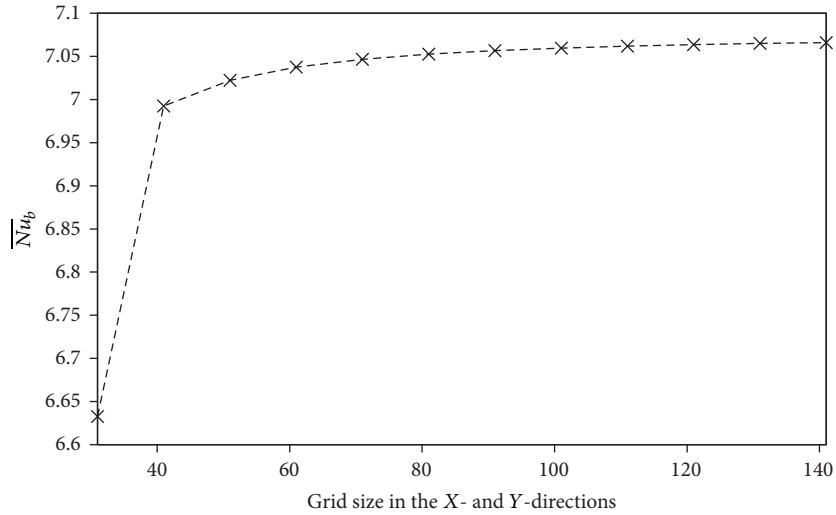

Figure 2: Grid independency study: $\overline{Nu_b}$ versus number of grid points.

Table 1: $|\Psi_{\min}^{\max}|$ against internal heating parameter with different K for continuous case at $\phi = 0.1$.

G	$K = 0$	$K = 2$	$K = 4$	$K = 6$
0.0	2.3522	1.2945	0.9082	0.6891
0.5	2.3519	1.3061	0.9269	0.7130
1.0	2.3482	1.3161	0.9448	0.7357
1.5	2.3401	1.3234	0.9610	0.7587
2.0	2.3233	1.3240	0.9723	0.7789

decrease of the strength convective flow circulation is with the increase of K. The reducing is more significant for lower values of G. The strengths of the convective flow circulation between Newtonian and micropolar liquid are different. The maximum flow magnitude decreases by increasing the internal heating parameter for the Newtonian liquid. However, maximum flow magnitude increases by increasing the internal heating parameter for the micropolar liquid ($K = 2, 4, 6$). The maximum flow strength of continuous heating case is slightly higher than the maximum flow strength of discontinuous heating case for the considered viscosity and internal heating parameters.

Figure 6 shows the variations of average Nusselt number at bottom (left) and average Nusselt number at side (right) against K by varying ϕ for continuous case 1 (top) and discontinuous heating case 2 (bottom) at $G = 1.0$. Apparently, as the nanoparticles concentration increases, the average Nusselt number at the bottom and side increases, revealing the significant role of the improved thermal properties of the nanoliquid in heat transport. The nanoparticles concentration modifies the heat transfer properties of the nanoliquid significantly. This is due to the fact that the thermal conductivity of the base liquid is weak and the addition of nanoparticles enhances the thermal conductivity of the nanoliquid. The microrotation effect is boosted in the low solid concentration and gets weaker as the concentration of the nanoparticles rises. Here it is doubted how the suppressing reaction of the microstructure on the thermal performance varies with the solid volume fraction. For each nanoparticles concentration, the effect of the material parameter was observed to suppress the thermal performance along the bottom and side wall for both cases, since an enhanced vortex viscosity increases the global viscosity of the liquid circulation, thus reducing the heat transfer rate. Indeed, the quadratic internal heating modifies the convective flow especially at the upper region.

An increase in material parameter reduces the average Nusselt number for cases 1 and 2 as shown in Figure 7. For both cases and fixed K, increasing the internal reaction decreases the heat transfer rate at the bottom but increases the heat transfer rate at the cool side. The continuous heating is observed to gain better thermal performance than the discontinuous heating case. This is due to the fact that the continuous thermal condition generates uniform heat along the heated plate that support the buoyancy. At the side cool wall, for $G = 0.5$, the heat transfer rate decreases by K, then after reaching a sufficiently large K value the heat transfer rate tends to be stagnant. This interesting result indicates that average Nusselt number at cool wall tends to be identical between Newtonian and micropolar nanoliquid for the weak internal heating at discontinuous heating case. This is due to the weak internal convective flow and nonuniform external convective flow being unable to produce the buoyancy.

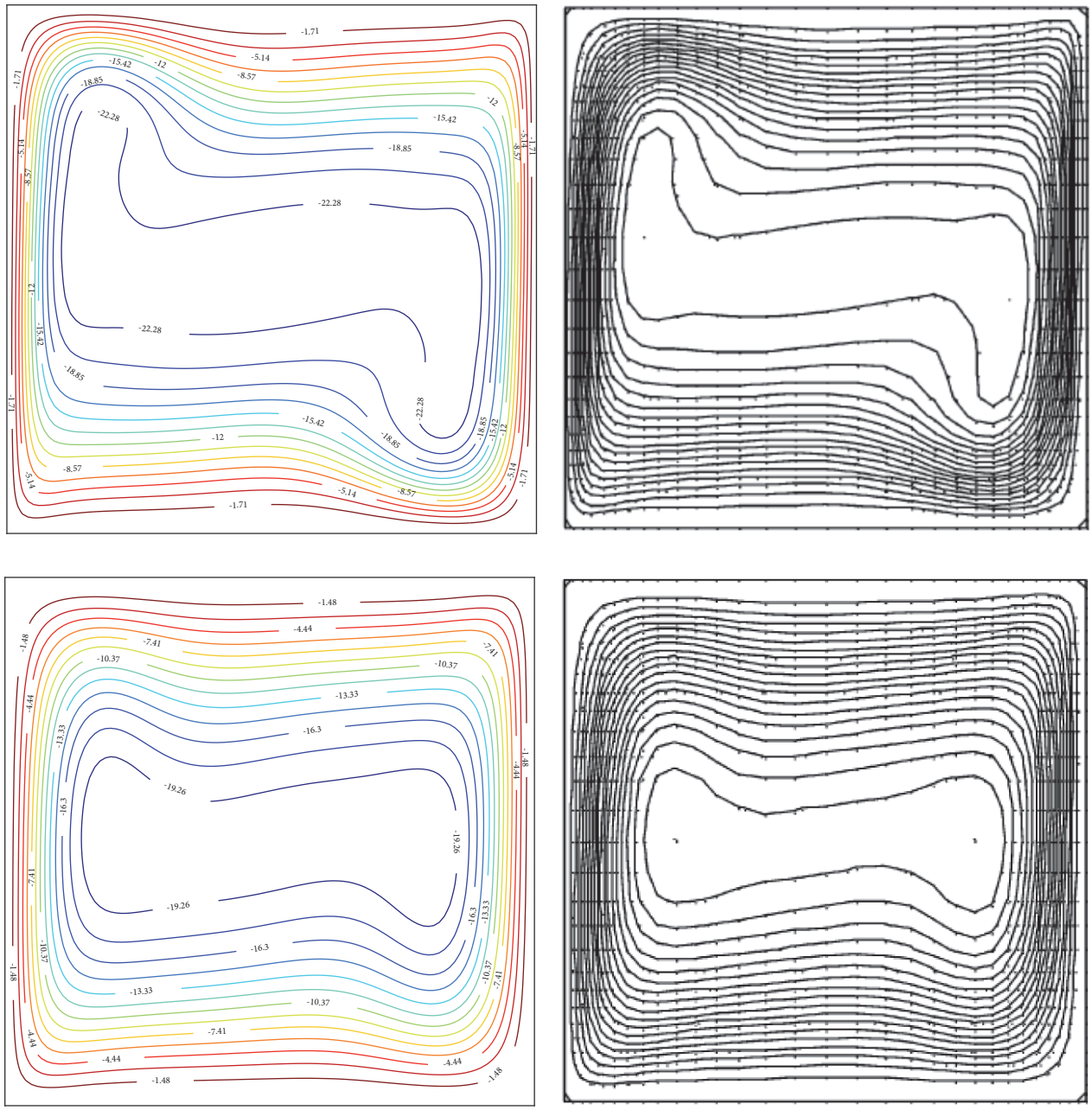

FIGURE 3: Comparison of computed streamlines with Aydin and Pop [10] results for continuous heating left wall at $\phi = 0$, $Ra = 10^6$, $Pr = 0.71$, $K = 0, 2$.

TABLE 2: $|\Psi_{\min}^{\max}|$ against internal heating parameter with different K for discontinuous case at $\phi = 0.1$.

G	$K = 0$	$K = 2$	$K = 4$	$K = 6$
0.0	2.1126	1.1531	0.8002	0.6003
0.5	2.1130	1.1631	0.8154	0.6186
1.0	2.1112	1.1721	0.8304	0.6373
1.5	2.1064	1.1796	0.8448	0.6566
2.0	2.0981	1.1848	0.8581	0.6786

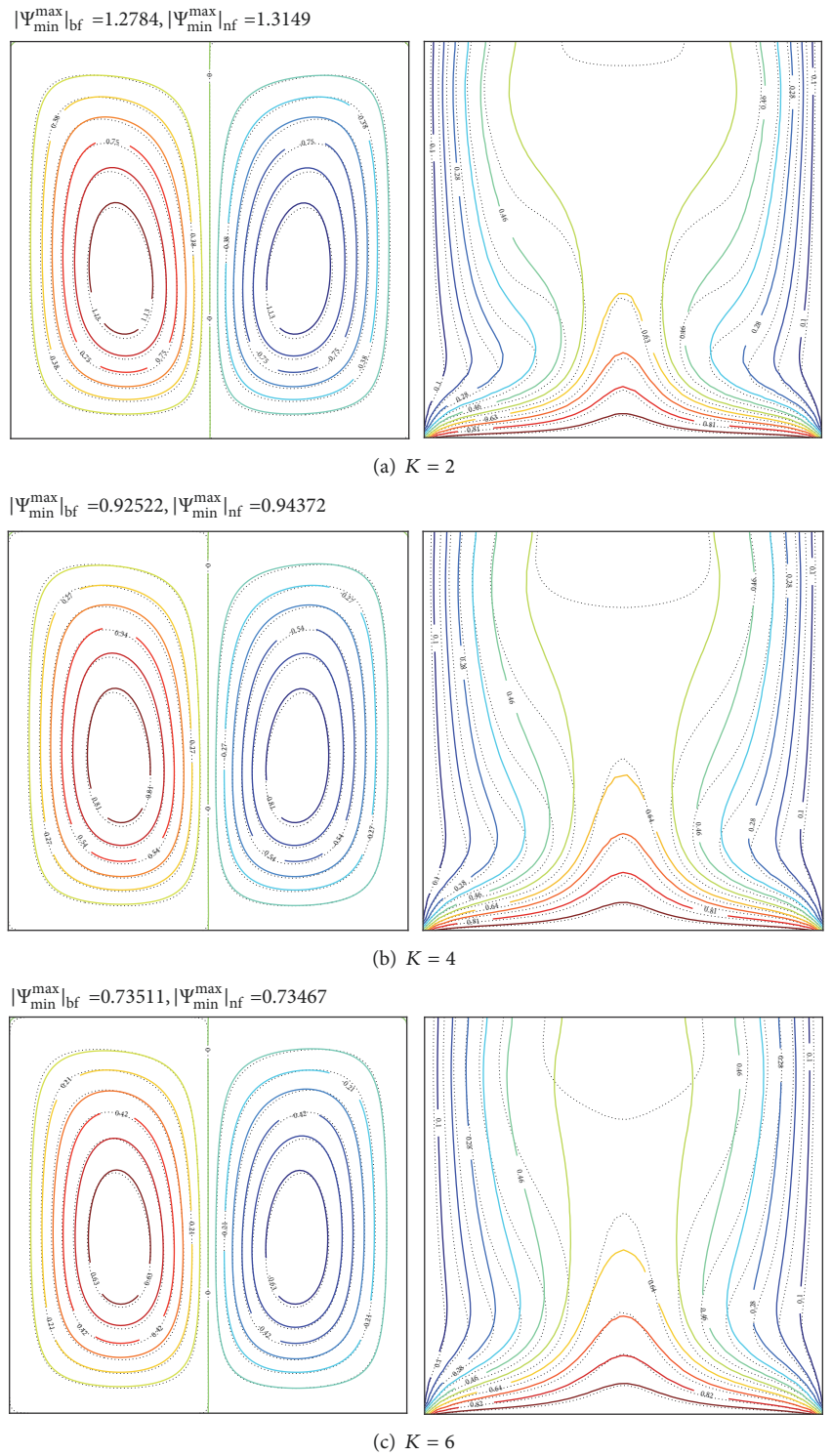

FIGURE 4: Streamlines and isotherms evolutions of nanoliquid (solid lines) and base liquid (dashed lines) by varying the material parameter for continuous heating corresponding to case 1 at $G = 1.0$.

5. Conclusions

The main purpose of the present research is to investigate the influence of continuous and discontinuous heating bottom surface and parabolic internal reaction profile on the liquid circulation, thermal distribution, and heat transfer characteristics due to convective heat transfer of micropolar nanoliquid. The dimensionless forms of the model equations

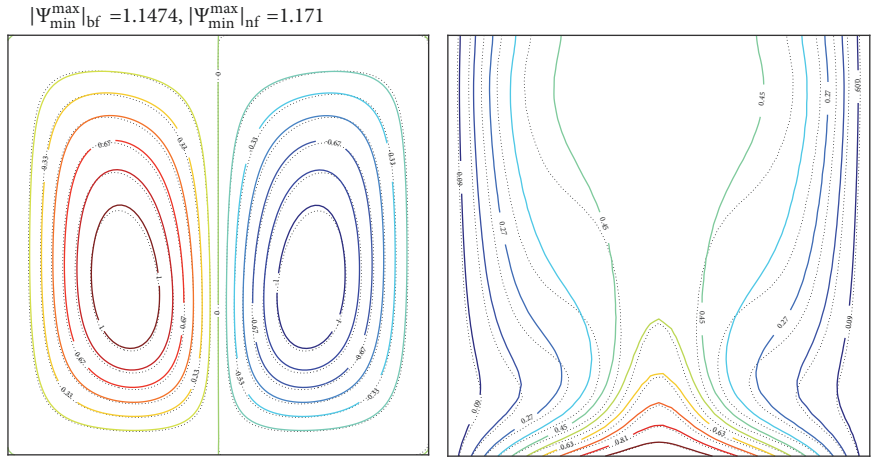

(a) $K = 2$

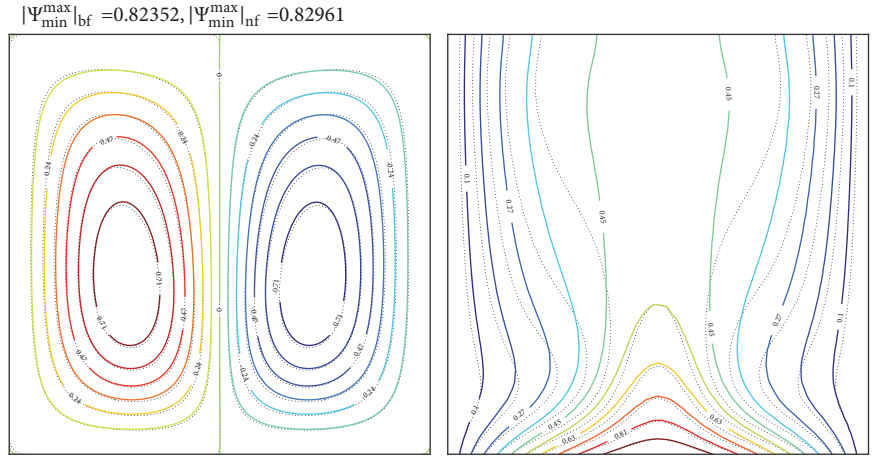

(b) $K = 4$

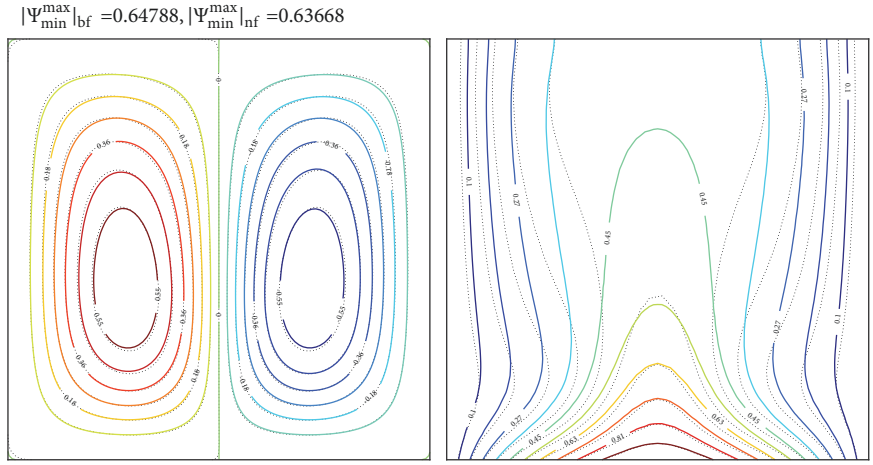

(c) $K = 6$

Figure 5: Streamlines and isotherms evolutions of nanoliquid (solid lines) and base liquid (dashed lines) by varying the material parameter for discontinuous heating corresponding to case 2 at $G = 1.0$.

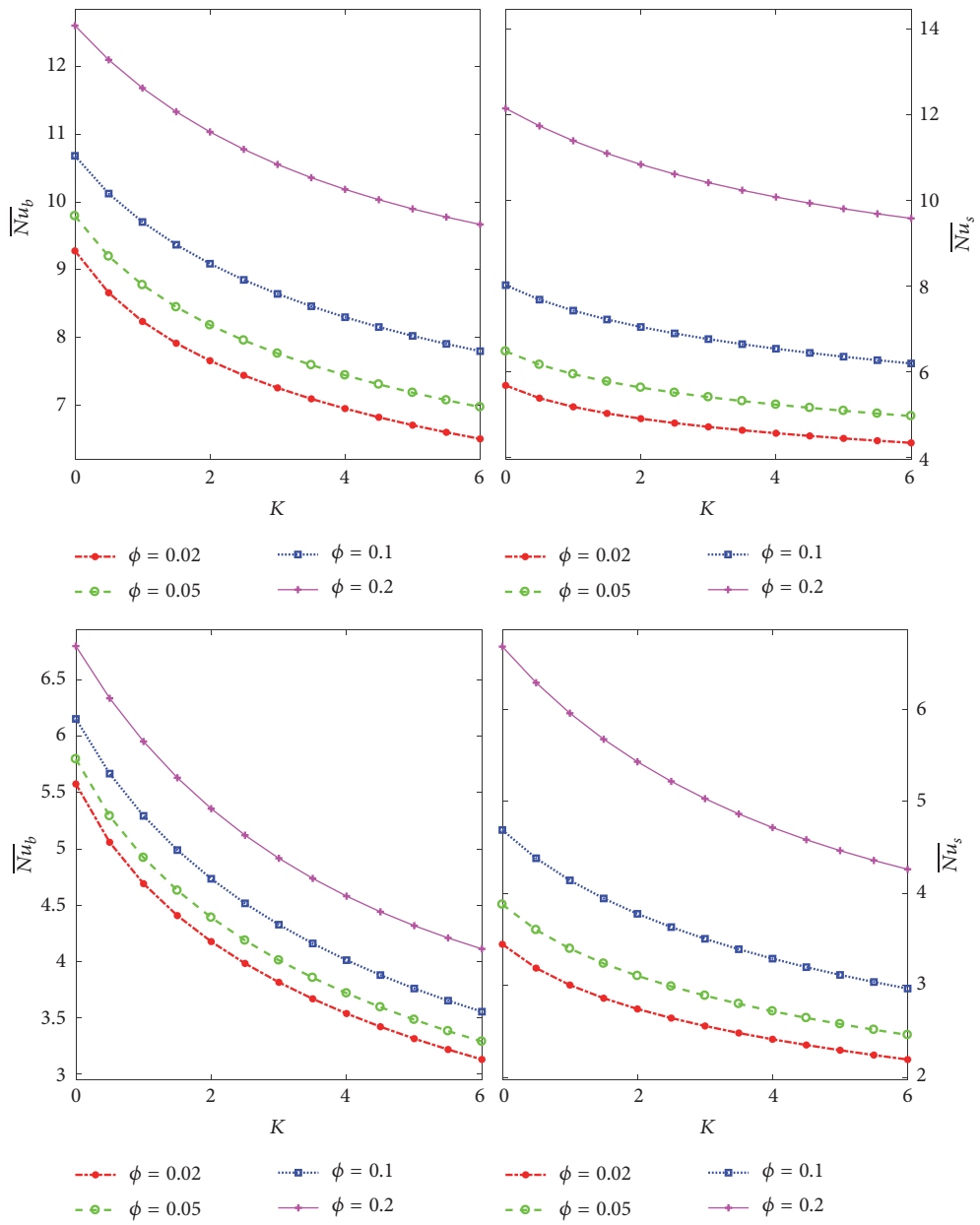

Figure 6: Variations of average Nusselt number at bottom (left) and average Nusselt number at side (right) against K by varying ϕ for continuous case 1 (top) and discontinuous heating case 2 (bottom) at $G = 1.0$.

are solved using the iterative finite difference technique. The important findings of the current analysis are as follows:

(1) The convective flow acceleration by adding nanoparticles is retarded by the microrotation and the suppression has a great impact on the weak exothermic reaction for both cases.

(2) In general, the heat transfers at hot and cool walls of micropolar nanoliquid are less than that of the Newtonian nanoliquid for both cases. The heat transfer at cool wall tends to be identical between Newtonian and micropolar nanoliquid for the weak exothermic reaction at discontinuous heating case.

(3) The heat transfer at hot and cool walls increases as the solid volume fraction of the nanoparticles increases for both cases.

(4) Increasing the internal reaction decreases the heat transfer at the hot wall but increases the heat transfer at the cool wall for both cases, Newtonian or micropolar nanoliquid.

Data Availability

The data used to support the findings of this study are included within the article.

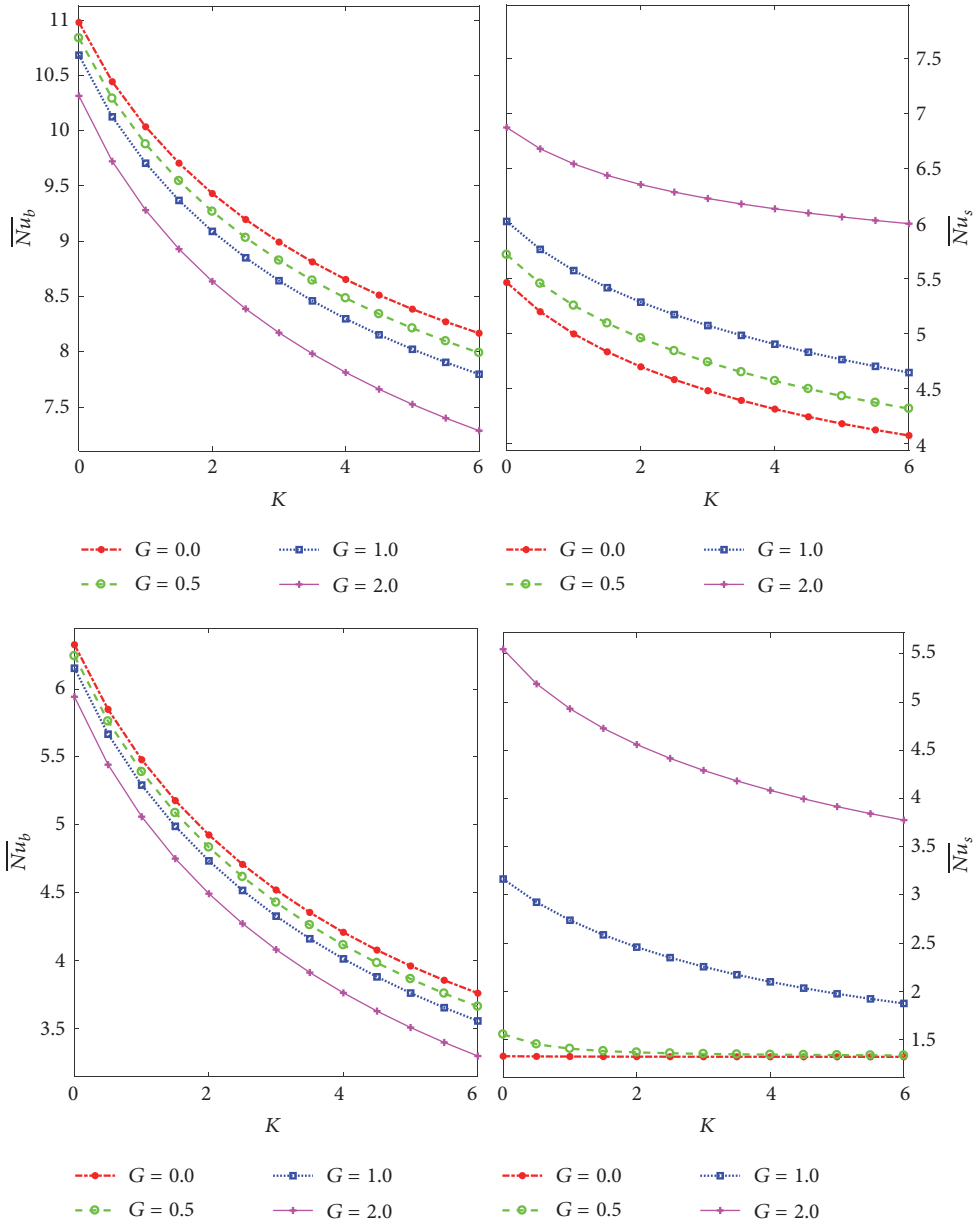

FIGURE 7: Variations of average Nusselt number at bottom (left) and average Nusselt number at side (right) against K by varying ϕ for continuous case 1 (top) and discontinuous heating case 2 (bottom) at $G = 1.0$.

Conflicts of Interest

The author declares there are no conflicts of interest regarding the publication of this paper.

References

[1] S. U. S. Choi, "Enhancing thermal conductivity of fluids with nanoparticles," in *Proceedings of the ASME International Mechanical Engineering Congress and Exposition*, pp. 99–105, November 1995.

[2] K. Khanafer, K. Vafai, and M. Lightstone, "Buoyancy-driven heat transfer enhancement in a two-dimensional enclosure utilizing nanofluids," *International Journal of Heat and Mass Transfer*, vol. 46, no. 19, pp. 3639–3653, 2003.

[3] R.-Y. Jou and S.-C. Tzeng, "Numerical research of nature convective heat transfer enhancement filled with nanofluids in rectangular enclosures," *International Communications in Heat and Mass Transfer*, vol. 33, no. 6, pp. 727–736, 2006.

[4] E. Büyük Öğüt, "Natural convection of water-based nanofluids in an inclined enclosure with a heat source," *International Journal of Thermal Sciences*, vol. 48, no. 11, pp. 2063–2073, 2009.

[5] W. Rashmi, A. F. Ismail, M. Khalid, and Y. Faridah, "CFD studies on natural convection heat transfer of Al_2O_3-water nanofluids," *Heat and Mass Transfer*, vol. 47, no. 10, pp. 1301–1310, 2011.

[6] G. A. Sheikhzadeh, M. Dastmalchi, and H. Khorasanizadeh, "Effects of nanoparticles transport mechanisms on Al2O 3-water nanofluid natural convection in a square enclosure," *International Journal of Thermal Sciences*, vol. 66, pp. 51–62, 2013.

[7] Z. Boulahia, A. Wakif, and R. Sehaqui, "Numerical study of mixed convection of the nanofluids in two-sided lid-driven square cavity with a pair of triangular heating cylinders," *Journal of Engineering (United States)*, vol. 2016, 2016.

[8] S. Y. Motlagh and H. Soltanipour, "Natural convection of Al2O3-water nanofluid in an inclined cavity using Buongiorno's two-phase model," *International Journal of Thermal Sciences*, vol. 111, pp. 310–320, 2017.

[9] C.-C. Liao, "Heat transfer transitions of natural convection flows in a differentially heated square enclosure filled with nanofluids," *International Journal of Heat and Mass Transfer*, vol. 115, pp. 625–634, 2017.

[10] O. Aydin and I. Pop, "Natural convection in a differentially heated enclosure filled with a micropolar fluid," *International Journal of Thermal Sciences*, vol. 46, no. 10, pp. 963–969, 2007.

[11] M. Saleem, S. Asghar, and M. A. Hossain, "Natural convection flow of micropolar fluid in a rectangular cavity heated from below with cold sidewalls," *Mathematical and Computer Modelling*, vol. 54, no. 1-2, pp. 508–518, 2011.

[12] S. K. Jena and S. P. Bhattacharyya, "The effect of microstructure on the thermal convection in a rectangular box of fluid heated from below," *International Journal of Engineering Science*, vol. 24, no. 1, pp. 69–78, 1986.

[13] S.-G. Wang and T.-H. Hsu, "Natural convection of micropolar fluids in an inclined rectangular enclosure," *Mathematical and Computer Modelling*, vol. 17, no. 10, pp. 73–80, 1993.

[14] T.-H. Tsu and C.-K. Chen, "Natural convection of micropolar fluids in a rectangular enclosure," *International Journal of Engineering Science*, vol. 34, no. 4, pp. 407–415, 1996.

[15] T.-H. Hsu, P.-T. Hsu, and S. O.-Y. Tsai, "Natural convection of micropolar fluids in an enclosure with heat sources," *International Journal of Heat and Mass Transfer*, vol. 40, no. 17, pp. 4239–4249, 1997.

[16] T. H. Hsu and K. Y. Hong, "Natural Convection of Micropolar Fluids in an Open Cavity," *Numerical Heat Transfer, Part A: Applications*, vol. 50, no. 3, pp. 281–300, 2006.

[17] N. S. Gibanov, M. A. Sheremet, and I. Pop, "Free convection in a trapezoidal cavity filled with a micropolar fluid," *International Journal of Heat and Mass Transfer*, vol. 99, pp. 831–838, 2016.

[18] I. V. Miroshnichenko, M. A. Sheremet, and I. Pop, "Natural convection in a trapezoidal cavity filled with a micropolar fluid under the effect of a local heat source," *International Journal of Mechanical Sciences*, vol. 120, pp. 182–189, 2017.

[19] M. A. Sheremet, I. Pop, and A. Ishak, "Time-dependent natural convection of micropolar fluid in a wavy triangular cavity," *International Journal of Heat and Mass Transfer*, vol. 105, pp. 610–622, 2017.

[20] O. Turk and M. Tezer-Sezgin, "FEM solution to natural convection flow of a micropolar nanofluid in the presence of a magnetic field," *Meccanica*, vol. 52, no. 4-5, pp. 889–901, 2017.

[21] N. Ali, M. Nazeer, T. Javed, and M. A. Siddiqui, "Buoyancy-driven cavity flow of a micropolar fluid with variably heated bottom wall," *Heat Transfer Research*, vol. 49, no. 5, pp. 457–481, 2018.

[22] G. C. Bourantas and V. C. Loukopoulos, "Modeling the natural convective flow of micropolar nanofluids," *International Journal of Heat and Mass Transfer*, vol. 68, pp. 35–41, 2014.

[23] H. Hashemi, Z. Namazian, and S. A. M. Mehryan, "Cu-water micropolar nanofluid natural convection within a porous enclosure with heat generation," *Journal of Molecular Liquids*, vol. 236, pp. 48–60, 2017.

[24] M. Izadi, S. Mehryan, and M. A. Sheremet, "Natural convection of CuO-water micropolar nanofluids inside a porous enclosure using local thermal non-equilibrium condition," *Journal of the Taiwan Institute of Chemical Engineers*, vol. 88, pp. 89–103, 2018.

[25] H. C. Brinkman, "The viscosity of concentrated suspensions and solutions," *The Journal of Chemical Physics*, vol. 20, no. 4, p. 571, 1952.